Crossref Similarity Check
Powered by iThenticate

*Reason- A Technical Journal*
ISSN 2277-1654
Volume XIX 2020

# RSM BASED MODELING AND OPTIMIZATION OF TIG WELDED JOINT

**Abhishek Ghosh[1], Sudip Mandal[2*], Goutam Nandi[3] and Pradip Kumar Pal[4]**

[1]Department of Mechanical Engineering, Jadavpur University, Kolkata- 700032.
Email: a.ghosh865@gmail.com
[2*]Department of Electronics and Communication Engineering, Jalpaiguri Govt. Engg. College, Jalpaiguri-735102.
Email:sudip.mandal007@gmail.com"
[3]Department of Mechanical Engineering, Jadavpur University, Kolkata- 700032.
Email: gnandi87@gmail.com
[4]Department of Mechanical Engineering, Jadavpur University, Kolkata- 700032.
Email: pradippal54@yahoo.com

Paper received on: August 05, 2020, accepted after revision on: April 21 2021
DOI:10.21843/reas/2020/94-111/209275

**Abstract:** Martensitic stainless steels are very difficult to weld. In this proposed work, effort is given on picking TIG welding optimum input parametric combination to join AISI 420 grade sheets. Welding current, shielding gas flow rate and welding (travel) speed are taken as input parameters. Whereas, ultimate tensile strength *(UTS)* and ductility *(D)* i.e. elongation of the weldment are considered as response or output parameters. Initially, response surface methodology (RSM) based face-centered central composite design (CCD) is employed for mathematical modeling by regression analysis. Next, six efficient metaheuristics and RSM optimization have been applied to maximize the output welding parameters. From the simulated results, the optimum parametric setting i.e. best set of welding current, gas flow rate and welding speed is identified in for maximization of UTS and D. Confirmatory tests are also conducted to validate the proposed approach.

**Keywords:** AISI 420 grade Martensitic stainless steel, homogeneous TIG welding, RSM modeling, Metaheuristic, Optimization.

## 1. INTRODUCTION

Martensitic stainless steels are ternary Fe-C-Cr alloy having body centric tetragonal (BCT) crystal structure [1]. It is difficult to weld them because martensite is hard, brittle and notch sensitive [2]. High shrinkage stress is generated during welding which along with thermal stress can cause high stress concentration if any physical defects present; crack propagates rapidly at fusion zone and HAZ [3, 4]**.** Abrupt decrease in solubility of hydrogen in martensite compared to austenite causes super saturation of hydrogen which results in liberation of molecular hydrogen at micro-defects. This can amplify local pressure and initiate local fracture even few hours after welding. This is called cold cracking. Presence of retained δ-ferrite in fusion zone has detrimental effects on quality of welded joints [5, 6]. All these factors make it difficult for engineers to produce defect free welding of martensitic stainless steels.

Grade AISI 420 is classified as medium carbon one, as it contain carbon percentage more than 0.15 % [2]. Presence of higher

carbon percentage in the grade makes preheating essential to avoid formation of crack during welding [3, 5]. Preheating above $M_s$ (martensitic start) temperature for few minutes markedly reduces post weld cooling rate, delays martensitic transformation, reduces notch sensitivity and stress concentration of martensite [4-6]. All these factors reduce the risk of brittle fracture post welding.

Few research papers are available in the literature, regarding welding of this grade of stainless steel. Kose and Kacar [4] welded 4 mm thick AISI 420 grades by $CO_2$ laser beam welding by giving pre-heat at 300°C for 60 minutes. Baghjari and Mousavi [6] made autogeneous butt joints of AISI 420 grades by pulsed Nd:YAG laser welding. Shirmohammadi et al. [8] and Pouranvari [9] attempted welding of 1.5 mm thick AISI 420 grade sheets by resistance spot welding process. Kurt et al [10] investigated effects of keyhole PTA (plasma transfer arc) welding process parameters when joining AISI 420 grade plates using interface of austenitic stainless steel. Yilmaz and Turkyılmazoglu [11] preferred TIG welding to join AISI 420 grades.

Earlier, few researchers [12-23] had utilized some statistical and computational intelligence techniques to enhance efficiency of several welding processes. Few methods such as RSM [13-16], Taguchi method [17-18], ANN [19-20], Fuzzy Logic [21] and Regression analysis [22-23] are found to be very effective in optimizing joint strength, bead geometry etc. and identifying the corresponding optimum input parametric combinations. Metaheuristic [24, 25] methods which are mainly inspired by physical phenomena, behavior of animals and evolutionary concepts, are widely used now-a-days for solving different real life optimization problems. And it is known that Genetic Algorithm (GA) [26-27] has been widely employed in optimizing welding problems.

Shortcomings of the welding process in the light of input parametric combinations reported till date in the literature, is the motivation of this research work. In this present work, attention has been given on selection of optimum TIG welding parameters so as to maximize the responses in joining AISI 420 grades, 2 mm thick. Welding current (I) welding speed (S) and shielding gas flow rate (F) have been taken as variable input welding parameters. These three welding parameters are considered because it is expected that they have much influence on heat input, arc characteristics etc. and also influence weld bead geometry, joint strength etc. For TIG welding, the shielding gas flow rate influences the arc stability which in turn decides the total heat input. Effects of welding parameters like stand-off distance, properties of electrode, working angle etc. on affecting the overall welding process are also overlooked.

Data of ultimate tensile strength *(UTS)* and ductility (% elongation, D) of the weldment extracted from tensile tests, have been used as output parameters. Then, mathematical models are generated by regression analysis using RSM method to relate output parameters (UTS and D) in terms of input parameters I, F and S. Next, regression equations have been used for multi-variable optimization by

RSM method and six recently proposed metaheuristic methods. The aim is to recognize the optimized parametric combination and the best optimization method to maximize the response parameters.

## 2. METHODOLOGY

This approach of RSM based metaheuristic optimization of TIG welding parametric combinations consists of three steps as follows: a) Completion of TIG welding and tensile tests b) Mathematical model building c) Implementation of different metaheuristics and RSM process to maximize the output parameters of TIG welding. In addition, metallurgical characteristics of the welded joint have been evaluated. All the steps are explained below:

### 2.1 Experimentation

2 mm thick sheets of grade AISI 420 at annealed condition are used for making square butt joints by TIG welding process in the present investigation. Chemical composition of the base metal is tested in laboratory and is shown in Table 1. Ultimate tensile strength, % elongation and hardness of the base metal have been measured to be 536.91 MPa, 13.14 % and 82.1 HRB respectively. Tensile stress-strain curve of the base metal is shown in Fig. 1. Input parameters and their levels have been shown in Table 2. Three levels are considered for each input parameter. The levels have been fixed based on experience of the expert welder, usual practices in the industry, authors' knowledge and perception along with several trial runs.

Twenty single pass welded joints have been made based on CCD design without edge preparation in 99% pure argon gas environment. Filler material for welding has been prepared in the laboratory from the base material. '$M_s$ Temperature' of the base metal is found to be 288.5° as calculated using Andrews' [7] empirical formula. Preheating has been given to the base metal at 300°C for 30 minutes.

After welding, samples are cut transversely from the joints in a wire-cut EDM and then mechanically ground (using grinding paper, 300-2000 mesh), polished (by 1µm diamond paste) and finally etched by aqua regia ($HCl:HNO_3$ = 3:1) solution. Specimens for tensile testing are made according to ASTM E8 standard, as shown in Fig. 2. LECO LM 248AT micro-hardness tester is employed to plot hardness profile of etched samples. DMLM/11888605 Leica metallurgical microscope is used for capturing digital images of microstructure. Fracture analysis of a broken tensile test specimen has been done using SEM (Jeol JSM-5510).

**Table 1:** Composition of the **AISI 420** sheet

| %C | %Cr | %Mn | %S | % Si | % Ni | % P | % Cu | Mo | % Fe |
|---|---|---|---|---|---|---|---|---|---|
| 0.19 | 12.68 | 0.45 | 0.007 | 0.28 | 0.17 | 0.032 | - | - | Rest |

**Table 2:** Input parameters and their levels

| Input parameters | Level 1 | Level 2 | Level 3 |
|---|---|---|---|
| Welding current (A) | 60 | 80 | 100 |
| Gas flow rate(L/min) | 9 | 12 | 15 |
| Travel speed(mm/s) | 1 | 1.5 | 2 |

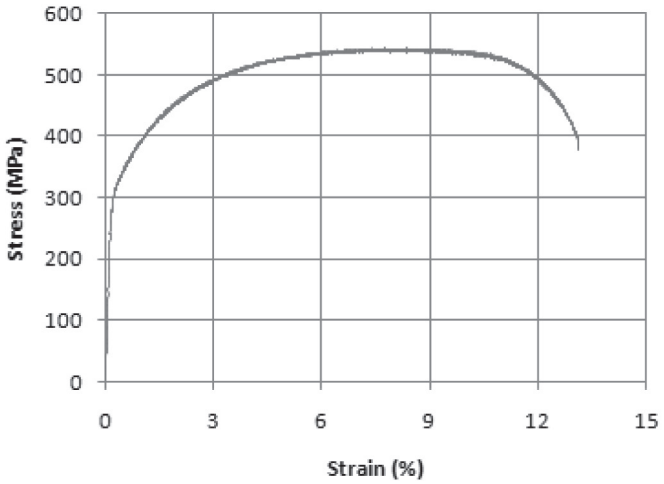


**Fig. 1.** Stress-strain curve of the base metal

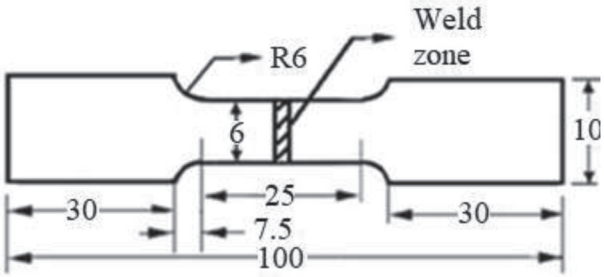


**Fig. 2.** ASTM E8 sub-size tensile specimen [25]

## 2.2 Numerical Modeling

Then mathematical models have been generated by regression analysis, based on Response Surface Methodology (RSM) to define the responses $UST$ and ductility in terms of welding parameters. RSM is frequently used for experimental modeling and analysis of it. It is mostly applied in problems where different input variables influence some outputs or response parameters. The response 'y' is a function of two variables $x_1$ and $x_2$. Now response y is written as following equation

$$y = f(x_1, x_2) + \varepsilon \quad (1)$$

where ε is random experimental error with zero mean. If one denotes the expected response by

$$E(y) = f(x_1, x_2) = \eta, \quad (2)$$

then the response surface can be denoted as $\eta = f(x_1, x_2)$. The response is represented graphically with the help of 3-D surface plots or 2-D contour plots. However, second order RSM models are commonly used when an approximation to the true response surface in a relatively small region is required. Moreover, second order models are more flexible and can take different forms as per the problem. A second order model is presented as

$$y = \beta_0 + \sum_{i=1}^{k} \beta_i x_i + \sum_{i=1}^{k} \beta_{ii} x_i^2 + \sum \sum_{i<j} \beta_{ij} x_i x_j + \varepsilon \quad (3)$$

where, $\beta_i$ 's are the regression coefficients and least squares method is used to estimate the regression coefficients ($\beta$'s) in the second order model. Desirability function [41] approach is generally used for multi-objective RSM optimization.

### 2.3 Parametric Optimization

Then, six metaheuristic methods are used for multivariable response optimization to identify the suitable parametric combinations of welding current, gas flow rate and welding speed such that the value of UST and Ductility become maximum. In the present research, six recently proposed metaheuristics namely Bat Algorithm (BA) [28-29], Cuckoo Search (CS) Algorithm [30-31], Flower Pollination Algorithm (FPA) [32-33], Particle Swarm Optimization (PSO) [34-35], Elephant Swarm Water Search Algorithm (ESWSA) [36-37, 42] and Genetic Algorithm [38-40] have been considered and validated against this present problem of modeling of welding process.

Bat Algorithm (BA) [28] follows the echolocation behavior of bats in search of prey with the help of changing loudness and frequency of the transmitted sound. Cuckoo Search [30] optimization is inspired from the brood parasitism behavior of cuckoo birds which lay their eggs by using the nests of other host birds. Flower Pollination Algorithm (FPA) [32] is based on the phenomenon of transfer of pollen for flowering of plants, and different pollinators like insects, birds and bats etc. helped for such transfer. PSO [34] optimization technique replicates the collective social movement of particles such as birds flocking. Depending on current best and global best positions, the velocity and position of the particles are updated. ESWSA [42] algorithm is inspired by water search (during drought) behavior of social elephants groups by using their sophisticated short and long distance communication techniques. GA [38] is another widely used optimization technique that follows the processes of natural evolution such selection, cross over, mutation and accepting.

Overall optimization process has three phases. First, metaheuristics search suitable values of $I$, $F$ and $S$ such that $UTS$ is maximized. Second, metaheuristics search a suitable values of $I$, $F$ and $S$ such that Ductility $(D)$ is $(UTS + D)$. Search dimension for each metaheuristic is 3. The objective functions are as follows:

$$f_a = Equation\ of\ UTS\ using\ RSM\ based\ regression\ analysis \quad (4)$$

$$f_b = Equation\ of\ Ductility\ (D)\ using\ RSM\ based\ regression\ analysis \quad (5)$$

$$f_c = |f_a| + |f_b| \quad (6)$$

This is another form of multi-objective optimization. Moreover, the results obtained

from the above mentioned metaheuristics are also compared to find the most efficient metaheuristic for this problem. All the simulations were performed in MATLAB R2013a Software using Windows7 Operating System, 2GB RAM and Duo-core processor.

## 3. RESULTS AND DISCUSSION

In this section, the results have been shown and discussed.

### 3.1 Tensile Test Data of Welded Joints

All welded joints are found sound in visual observation. Next, tensile test of welded samples has been carried out. UTS and % elongation data of all the welded samples are recorded and are also enlisted in Table 3. Strength and ductility of three butt joints (sample No. 1, 4 and 8) are found to be non-satisfactory. On examination it is found that the sample No. 1, 2, 3, 4, 6, 7, 8, 10, 12, 15 and 18 have failed through the fusion zone and rest of the samples failed from the base metal zone. In so far as ultimate tensile strength of the welded joints is concerned, it is within the range 485.8 MPa– 533.76 MPa. Sample No. 11, 14 and 19 show high ultimate tensile strength in tensile test. Few samples (sample No. 1, and 8) found to have lower strength. Elongation of the welded specimens in tensile test found to be satisfactory, ranging from 13.13 %- 17.81 %. The heighest value of ductility (% elongation) has been observed for sample No. 10 (17.81 %). Sample No. 1 is found to be least ductile. Tensile stress-strain curves of 2 samples (Sample No. 4 and 13) are shown in Fig. 3, as representative ones.

**Table 3:** Experimental design and responses

| Sl. No. | Input parameters | | | Output parameters | |
|---|---|---|---|---|---|
| | *I* (A) | F (L/min) | S (mm/s) | UTS (MPa) | % Elongation (Ductility) |
| 1 | 60 | 9 | 1.0 | 498.21 | 13.13 |
| 2 | 100 | 9 | 1.0 | 503.49 | 17.22 |
| 3 | 60 | 15 | 1.0 | 502.35 | 17.35 |
| 4 | 100 | 15 | 1.0 | 485.8 | 13.6 |
| 5 | 60 | 9 | 2.0 | 511.68 | 15.88 |
| 6 | 100 | 9 | 2.0 | 501.93 | 17.65 |
| 7 | 60 | 15 | 2.0 | 504.97 | 17.01 |
| 8 | 100 | 15 | 2.0 | 492.49 | 15.97 |
| 9 | 60 | 12 | 1.5 | 517.48 | 15.74 |
| 10 | 100 | 12 | 1.5 | 502.67 | 17.81 |
| 11 | 80 | 9 | 1.5 | 533.03 | 17.55 |
| 12 | 80 | 15 | 1.5 | 505.47 | 15.16 |
| 13 | 80 | 12 | 1.0 | 533.76 | 16.58 |
| 14 | 80 | 12 | 2.0 | 527.27 | 17.33 |
| 15 | 80 | 12 | 1.5 | 522.33 | 15.22 |
| 16 | 80 | 12 | 1.5 | 520.01 | 14.53 |
| 17 | 80 | 12 | 1.5 | 525.06 | 14.45 |
| 18 | 80 | 12 | 1.5 | 521.03 | 16.67 |
| 19 | 80 | 12 | 1.5 | 530.59 | 16.17 |
| 20 | 80 | 12 | 1.5 | 526.98 | 17.34 |

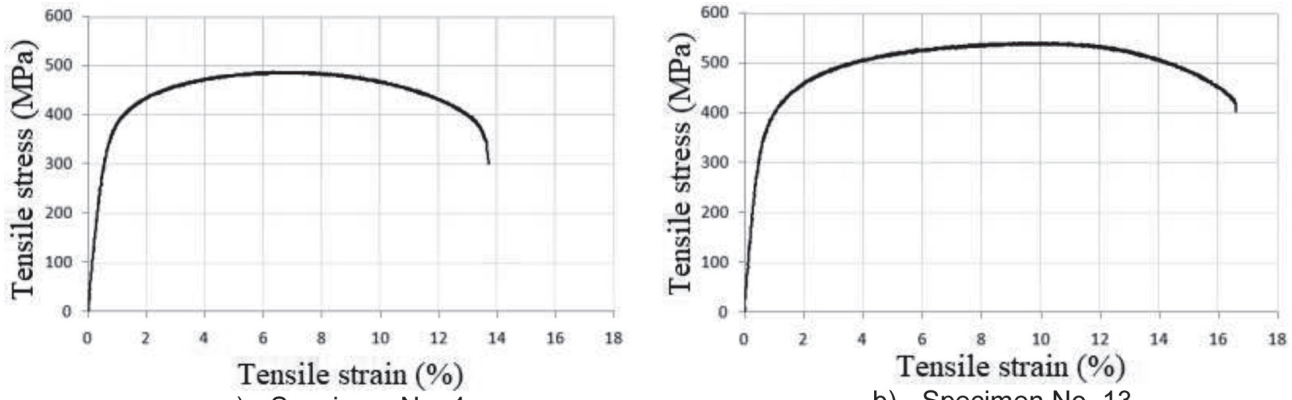


a) Specimen No. 4 b) Specimen No. 13

**Fig. 3.** Stress-strain curve of welded joints

### 3.2 Metallurgical Investigation of Welded Specimens

Few amount of retained δ-ferrite in martensitic matrix have been found in the fusion zone of most of the specimens. Full transformation of high temperature austenite into martensite is observed post solidification. Two representative images of microstructures of welded sample (sample No. 12) have been given in Fig. 4.

Equiaxed dendritic regions are found predominant in the fusion zone and HAZ of welded specimens. Chains of delta ferrite are also visible in fusion zone of most of the specimens. Rapid cooling rate of welding process may have prevented precipitation of carbides in fusion zone in most of the specimens. Dual phase microstructure composed of carbide in the matrix of martensite is found predominant in the HAZ region. Grain growth has been observed in HAZ region compared to base metal region. No significant effects of the rate of heat input (due to change in parametric combinations) on microstructure have been identified.

Hardness of the welded samples has been measured and the effects of heating and subsequent solidification cycle on hardness have been discussed. In the present study, non-uniform hardness profile is found; hardness of fusion zone and HAZ is found to be much higher than that of base metal. Hardness profile of sample No. 4 and 13 have been given in Fig. 5a and Fig. 5b respectively. Average hardness values of HAZ, fusion zone and base metal are found to be 445.49 HV, 465.6 HV and 159 HV respectively under loads of 50 g and at a dwell time of 10s. Small variations in fusion zone hardness may be due to presence of ferrite in grain boundaries. Ratio of fusion zone hardness to base metal hardness is 2.93. Carbide precipitation in HAZ has created dual phase microstructure composed of martensite plus carbide and attributed to high HAZ hardness. Absence of tampered martensite in HAZ prevents any fall in HAZ hardness.

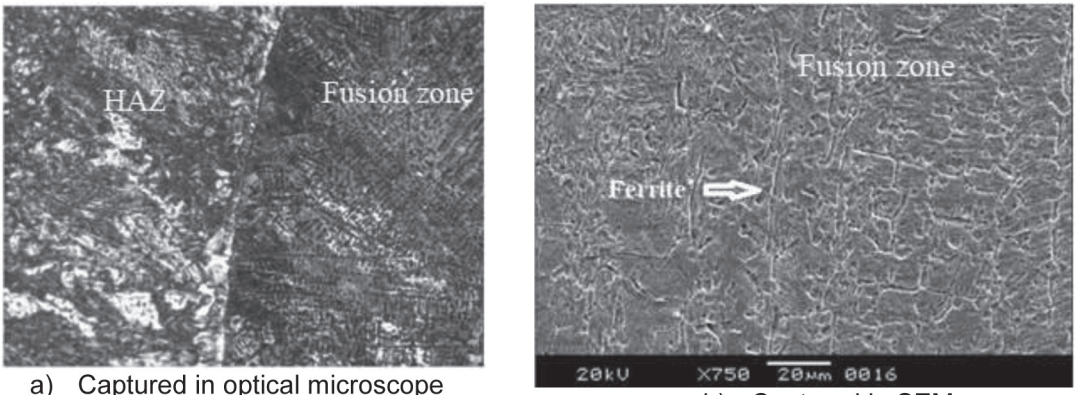


a) Captured in optical microscope

b) Captured in SEM

**Fig. 4.** Microstructure of specimen 12

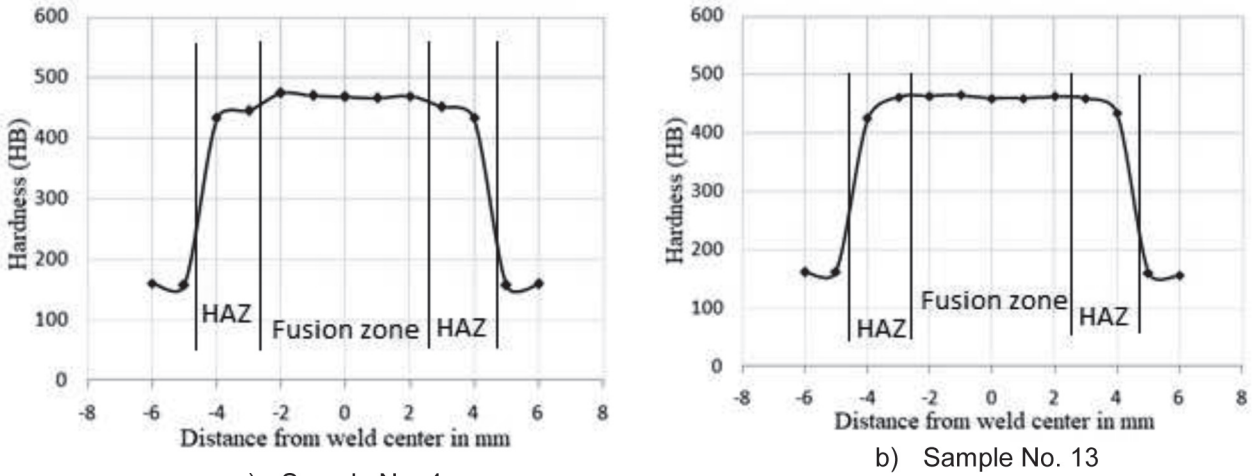


a) Sample No. 4

b) Sample No. 13

**Fig. 5.** Hardness profiles of welded joints

Mixture of ductile and brittle mechanisms has been observed from tensile fractured surfaces. Spherical particles in the centers of micro voids are not clear. Some secondary voids are present at the carbide interfaces. Slips in the fractured surfaces are observed in few cases. Representative SEM image of tensile fractured surface of sample No. 4 has been given in Fig. 6.

Due to low impact strength of the fusion zone, depth of the voids become shallow and cleavage planes increase. Strength mismatch, in high degree, between fusion zone and annealed martensitic stainless steel base metal produced strain localization in the fusion zone that promoted some plastic deformation before failure. Imbalance in mechanical properties between delta ferrite and the martensite along with lack of cohesion between the ferrite and the surrounding matrix suggest reduction in the toughness of the weldment significantly. It reduces chances of promoting brittle crack propagation into the fusion zone. Dissolution of chromium (Cr) rich carbides in carbon (C)

rich martensite matrix produced a brittle structure in HAZ which would offer an easy-crack growth path during loading.

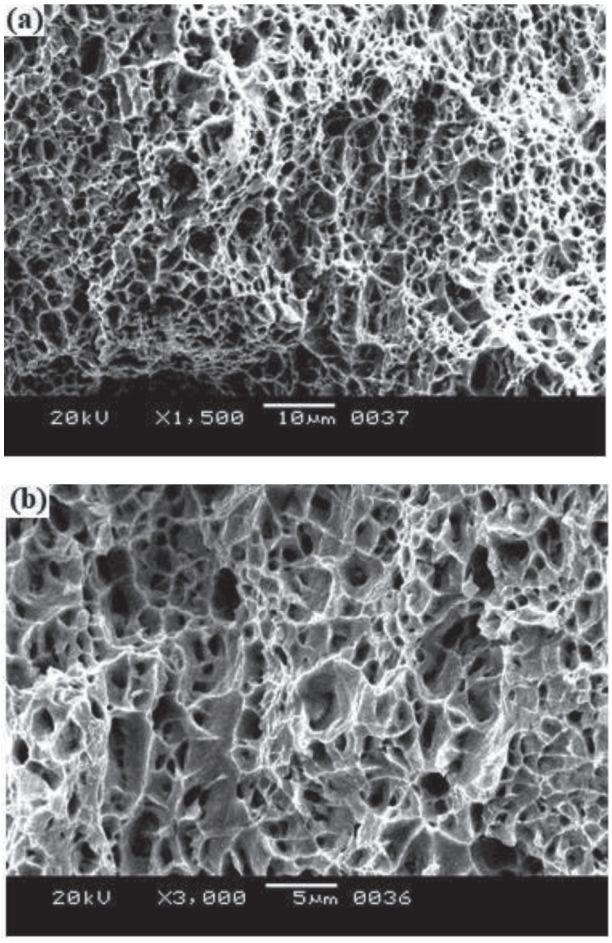


**Fig. 6.** Fractured surfaces of specimen 4

### 3.3 Mathematical Models of Responses (UTS and D)

Second order mathematical models (UTS & $D$) (regression equations) of both the responses are developed using MINITAB-16.1 software. The regression equations for ultimate tensile strength (UTS) and ductility (D) of the welded joint have been shown in Eq. (7) and (8) respectively.

$$UTS = 75.6 + 7.89 * I - 26.8 * F + 9.4 * S - 0.04570 * I * I - 1.012 * F * F + 8.6 * S * S - 0.0512 * I * F - 0.137 * I * S - 0.22 * F * S \quad (7)$$

$$D = -10.2 + 0.242 * I + 2.74 * F - 1.2 * S + 0.0002 * I * I - 0.0376 * F * F + 1.05 * S * S - 0.02219 * I * F + 0.0049 * I * S - 0.096 * F * S \quad (8)$$

In Fig. 7, comparison between measured responses and predicted responses by RSM method has been shown. Predicted responses are calculated from regression equations. Percentage deviation for response UTS is within ± 2 % and for response ductility within 10%.

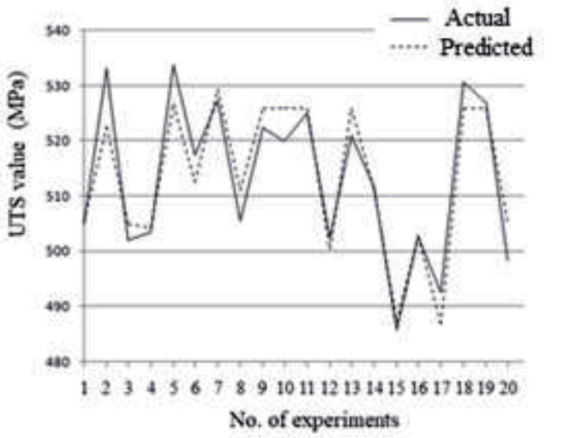


a) Response UTS

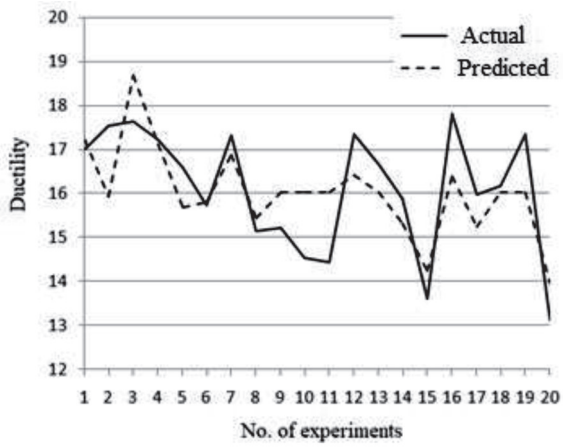


b) Response Ductility (D)

**Fig. 7.** Comparison of measured and predicted responses

ANOVA table for response UTS and ductility (D) have been shown in Table 4 and 5 respectively. From Table 4 it is observed that, gas flow rate (F) is the most significant factor affecting the response UTS having P value 0.018, followed by welding current (I) (P = 0.039). Travel speed (S) (P = 0.354) has no statistical significance on the response UTS. I-I (P = 0.001) and F-F (P = 0.041) are statistically significant inner-interaction terms but S-S (P = 0.590) is not statistically significant on the response. None of the cross-interaction terms, i.e., I-F (P = 0.207), F-S (P = 0.560) and I-S (P = 0.889) are significant. The determination factor R2 of this model is 89.23 %. This indicates that the proposed model is adequate. Adjusted R2 value of the model is 79.53 %.

**Table 4:** ANOVA table for response UTS

| Source | DF | Adj SS | Adj MS | F-Value | P-Value |
|---|---|---|---|---|---|
| **Model** | 9 | 3426.31 | 380.701 | 9.20 | 0.001 |
| **Linear** | 3 | 582.95 | 194.318 | 4.70 | 0.027 |
| **I** | 1 | 233.39 | 233.386 | 5.64 | 0.039 |
| **F** | 1 | 327.87 | 327.871 | 7.93 | 0.018 |
| **S** | 1 | 21.70 | 21.697 | 0.52 | 0.486 |
| **Square** | 3 | 2752.10 | 917.367 | 22.18 | 0.000 |
| **I-I** | 1 | 918.89 | 918.890 | 22.21 | 0.001 |
| **F-F** | 1 | 227.96 | 227.955 | 5.51 | 0.041 |
| **S-S** | 1 | 12.84 | 12.836 | 0.31 | 0.590 |
| **Interaction** | 3 | 91.26 | 30.420 | 0.74 | 0.554 |
| **I-F** | 1 | 75.40 | 75.399 | 1.82 | 0.207 |
| **I-S** | 1 | 15.02 | 15.015 | 0.36 | 0.560 |
| **F-S** | 1 | 0.85 | 0.845 | 0.02 | 0.889 |
| **Error** | 10 | 413.64 | 41.364 | | |
| **Lack-of-Fit** | 5 | 333.34 | 66.669 | 4.15 | 0.072 |
| **Pure Error** | 5 | 80.30 | 16.059 | | |
| **Total** | 19 | 3839.95 | | | |

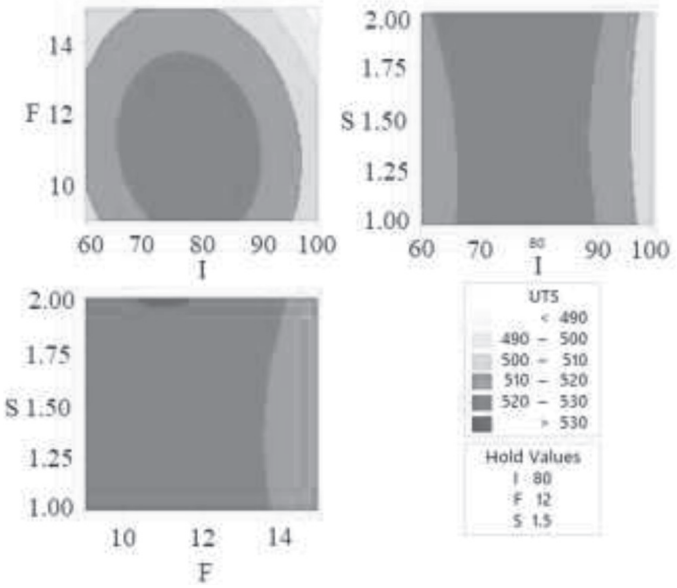


**Fig. 8.** Contour plots for response UTS

**Table 5:** ANOVA table for response % Elongation (D)

| Source | DF | Adj SS | Adj MS | F-Value | P-Value |
|---|---|---|---|---|---|
| **Model** | 9 | 19.8271 | 2.2030 | 1.30 | 0.343 |
| **Linear** | 3 | 5.0857 | 1.6952 | 1.00 | 0.433 |
| **I** | 1 | 0.9860 | 0.9860 | 0.58 | 0.463 |
| **F** | 1 | 0.5476 | 0.5476 | 0.32 | 0.582 |
| **S** | 1 | 3.5522 | 3.5522 | 2.09 | 0.178 |
| **Square** | 3 | 0.3793 | 0.1264 | 0.07 | 0.972 |
| **I-I** | 1 | 0.0184 | 0.0184 | 0.01 | 0.919 |
| **F-F** | 1 | 0.3145 | 0.3145 | 0.19 | 0.676 |
| **S-S** | 1 | 0.1885 | 0.1885 | 0.11 | 0.746 |
| **Interaction** | 3 | 14.3621 | 4.7874 | 2.82 | 0.093 |
| **I-F** | 1 | 14.1778 | 14.1778 | 8.36 | 0.016 |
| **I-S** | 1 | 0.0190 | 0.0190 | 0.01 | 0.918 |
| **F-S** | 1 | 0.1653 | 0.1653 | 0.10 | 0.761 |
| **Error** | 10 | 16.9624 | 1.6962 | | |
| **Lack-of-Fit** | 5 | 9.9546 | 1.9909 | 1.42 | 0.355 |
| **Pure Error** | 5 | 7.0078 | 1.4016 | | |
| **Total** | 19 | 36.7895 | | | |

The relationship between response UTS and the welding parameters has been illustrated by two dimensional graphs or contour plots in Fig. 8. Three plots, i.e., F vs. I, S vs. I and S vs. F have been shown keeping the third parameters constant at middle operating levels.

From Table 5 it is seen that, none of the linear terms, i.e., welding current (P = 0.463), gas flow rate (P = 0.582) and travel speed (P = 0.178) are significant on the response ductility (D). Inner-interaction terms, i.e., I-I (P = 0.919), F-F (P = 0.676) and S-S (P = 0.746) are also not significant. Among the cross-

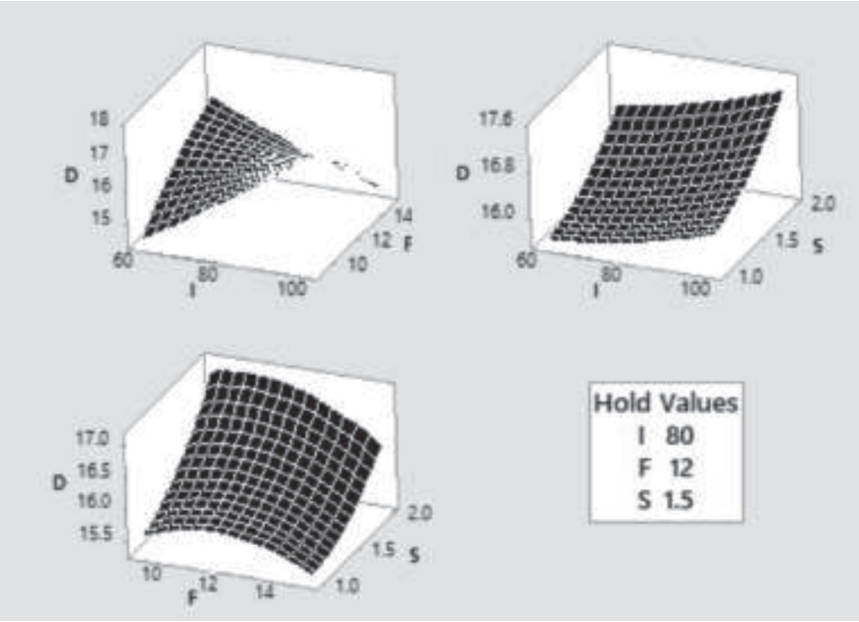


**Fig. 9.** Surface plots for response ductility (D)

interaction terms, I-F (P = 0.016) is found to be significant but I-S (P = 0.918) and F-S (P = 0.761) are not significant. R2 value of this model is 53.89 %.

The relationship between response ductility (D) and the welding parameters has been illustrated by three dimensional graphs or surface plots in Fig. 9. Three plots i.e., F vs. I, S vs. I and S vs. F are shown keeping the third parameters constant at middle operating levels.

### 3.4 Optimization of Responses

In this section, results of multi-variable optimization of responses by RSM method and six metaheuristic methods i.e. bat algorithm (BA), cuckoo search (CS) algorithm, flower pollination algorithm (FPA), particle swarm optimization (PSO) algorithm, elephant swarm water search algorithm (ESWSA) and genetic algorithm (GA) have been presented. Regression equations (Eq. (7) and (8)) developed by RSM method have been used as objective functions.

In Fig. 10, results of multi-objective optimization of responses ultimate tensile strength (UTS) and ductility (D) by RSM method has been shown. The aim is to maximize both the responses under operating ranges of input parameters. The optimized value of UTS is 528.94 MPa with desirability = 0.90 and the optimized value of ductility (D) is 17.26 % with desirability = 0.88. The optimized parametric combination is current I = 83.43 A, gas flow rate F = 10.45 l/min and travel speed S = 2.0 mm/s.

From Table 6, it is clear that CS, FPA, PSO and ESWSA are able to reach a maximum $I$ = 77.11 to 77.12 A, $F$ = 11.07 LPM and $S$ = 2.00 mm/s. BA and GA stuck into local optima but reach closer to it. On the other hand, from Table 7, it is found that all metaheuristics can reach the global maxima point of ductility i.e. 18.6954% at optimum parametric combination of $I$ = 100 A, $F$ = 9 LPM, $S$ = 2.00 mm/s.

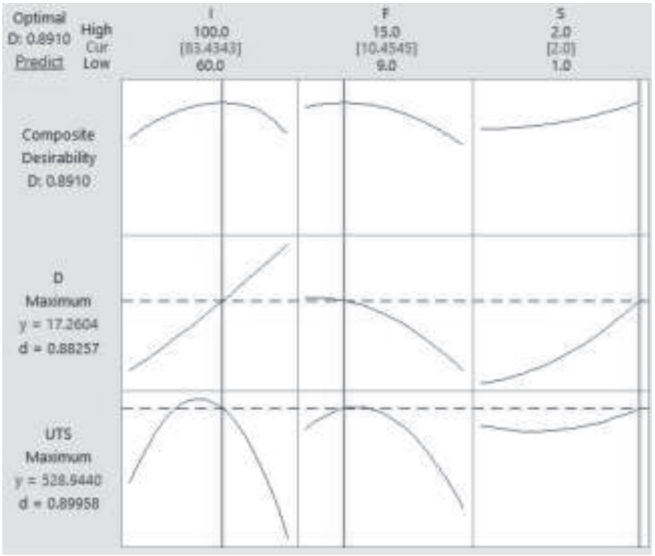


**Fig. 10.** Multi-objective optimization by RSM method

**Table 6**: UTS optimization using metaheuristics (simulation results)

| Metaheuristics | Best Fitness $f_{min}$ | Optimized Value of UTS | Optimized parametric combination | | |
|---|---|---|---|---|---|
| | | | I | F | S |
| BA | 0.001883936 | 530.803 | 77.8103 | 11.0525 | 2.0000 |
| CS | 0.001883860 | 530.825 | 77.1234 | 11.0728 | 2.0000 |
| FPA | 0.001883860 | 530.825 | 77.1190 | 11.0736 | 2.0000 |
| PSO | 0.001883860 | 530.825 | 77.1234 | 11.0728 | 2.0000 |
| ESWSA | 0.001883860 | 530.825 | 77.1234 | 11.0728 | 2.0000 |
| GA | 0.001883883 | 530.818 | 77.0000 | 11.0000 | 2.0000 |

**Table** 7: Results of simulation for optimization of response % elongation (D) using metaheuristics

| Metaheuristics | Best Fitness $f_{min}$ | Optimized Value of Ductility ($D$) | Optimized parametric combination | | |
|---|---|---|---|---|---|
| | | | I | F | S |
| BA | 0.053489 | 18.6954 | 100.0000 | 9.0000 | 2.0000 |
| CS | 0.053489 | 18.6954 | 100.0000 | 9.0000 | 2.0000 |
| FPA | 0.053489 | 18.6954 | 100.0000 | 9.0000 | 2.0000 |
| PSO | 0.053489 | 18.6954 | 100.0000 | 9.0000 | 2.0000 |
| ESWSA | 0.053489 | 18.6954 | 100.0000 | 9.0000 | 2.0000 |
| GA | 0.053489 | 18.6954 | 100.0000 | 9.0000 | 2.0000 |

**Table 8:** Simulation results for combined function of responses $UTS$ and % Elongation (D) optimization using metaheuristics

| Metaheuristics | Best Fitness $f_{min}$ | Optimized Value of Combined function of UTS and D | Optimized parametric combination | | |
|---|---|---|---|---|---|
| | | | I | F | S |
| BA | 0.001826457 | 547.50804 | 75.4818 | 11.1498 | 2.0000 |
| CS | 0.001825831 | 547.69559 | 77.5395 | 11.0601 | 2.0000 |
| FPA | 0.001825831 | 547.69558 | 77.5407 | 11.0577 | 2.0000 |
| PSO | 0.001825831 | 547.69559 | 77.5396 | 11.0601 | 2.0000 |
| ESWSA | 0.001825831 | 547.69559 | 77.5395 | 11.0601 | 2.0000 |
| GA | 0.001825869 | 547.68418 | 78.0000 | 11.0000 | 2.0000 |

Table 8 shows that for multi-objective optimi-zation of UTS and ductility simultaneously, CS, PSO and ESWSA show a maximal $\mathrm{USD} + \mathrm{D}$ point, i.e. 547.69559, for the optimal combination point, i.e. 547.69559, for the optimal combination $\mathrm{I}$ = 77.5396 A, $\mathrm{F}$ = 11.0601LPM, $\mathrm{S}$ = 2.00 mm/s. But BA and GA fail to reach global maxima. The optimal parametric conditions for present problem of TIG welding can be taken as $\mathrm{I}$ = [77, 100], $\mathrm{F}$ = [9, 12] $\mathrm{S}$ = 2.00. PSO perform better in term of reaching global maxima point i.e. reaching optimal condition for welding.

Table 9 shows average execution time taken by different metaheuristic methods for optimization of response $\mathrm{UTS}$. It is clear that GA is worst whereas PSO is best metaheuristic method in terms of execution time.

**Table 9:** Execution time for optimization by six methods

| Metaheuristics | Execution Time (s) for UTS | Execution Time (s) for D | Execution Time (s) for UTS + D |
|---|---|---|---|
| BA | 0.190412 | 0.247968 | 0.251268 |
| CS | 0.320495 | 0.342487 | 0.409071 |
| FPA | 0.248932 | 0.250424 | 0.252131 |
| PSO | 0.134753 | 0.153154 | 0.140134 |
| ESWSA | 0.152445 | 0.161137 | 0.160951 |
| GA | 6.022549 | 4.209095 | 8.805017 |

Fig. 11, 12 and 13 show convergence curve of different metaheuristics while optimizing the response D, UTS, and D+UTS respectively. Though here the iteration number is set to 1000, convergence up to 20$^{th}$ iteration is shown. All algorithms have converged to their optimal point within 20 iterations. It is clear that FPA converges faster than other methods for optimization of response ductility and PSO comes next. On the other hand, PSO is better for both UTS, and D+UTS optimization in term of convergence speed.

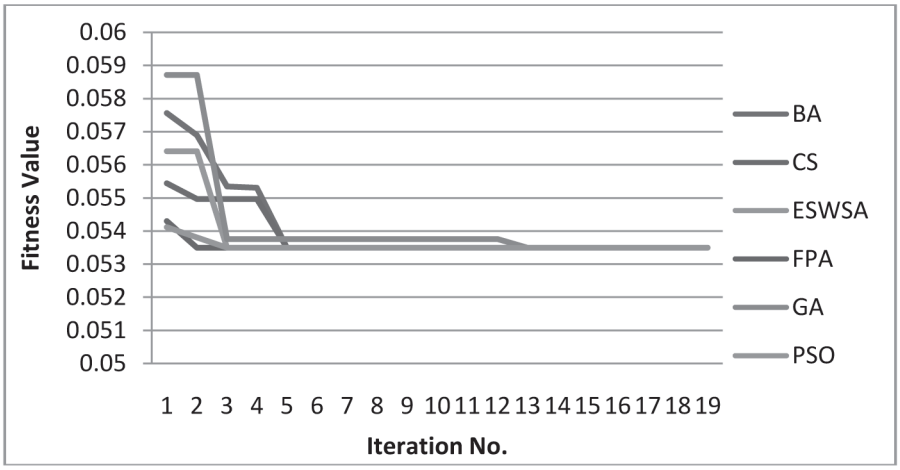


**Fig. 11.** Convergence curve for optimization of response % Elongation $(D)$

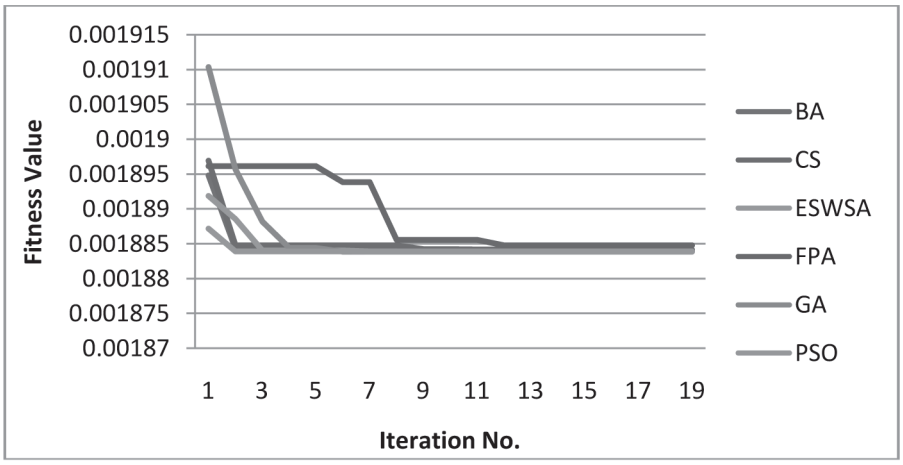


**Fig. 12.** Convergence curve for optimization of response UTS

Considering all that have been discussed above, it can be remarked that PSO algorithm is most suitable in terms of finding global optimization, as well as it is less time consuming and fast convergence (for most of the cases). For the present problem, the optimal parametric combination for maximum UTS and % Elongation (D), individually are taken as I = 77.12 A, F = 11.07 LPM, S =2.00 mm/s and I = 100 A, F = 9 LPM, S = 2 mm/s respectively. The corresponding values of UTS and % Elongation (D) at optimized parametric conditions are 530.825 MPa and 18.6954 % respectively.

Confirmatory tests have been conducted at optimal condition proposed by RSM method and PSO method to validate the simulation results. So, another two experiments of TIG welding have been performed to observe the experimental values of UTS and % Elongation (D) at optimal parametric conditions. From Table 10, it is also found that errors in simulated result are negligible (i.e. 0.07 % and 0.48 % error for UTS and % Elongation respectively). It strongly validates the proposed methods of optimization.

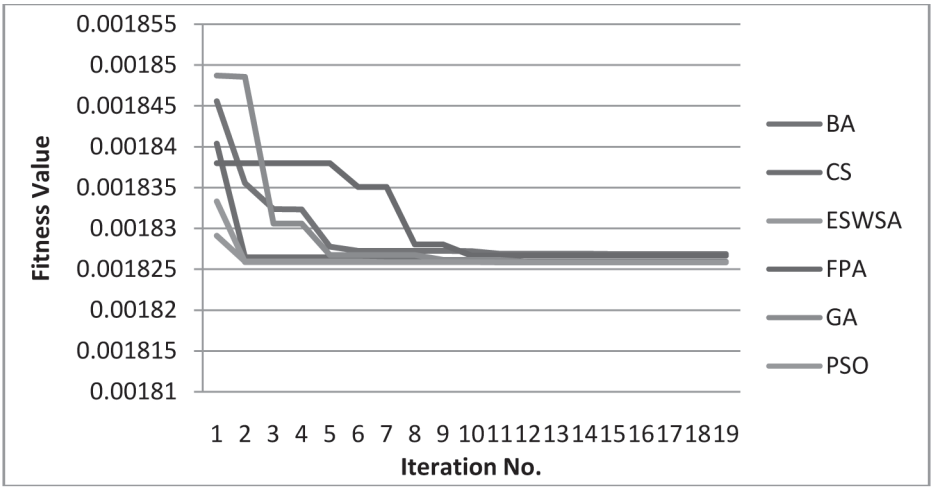


**Fig. 13.** Convergence curve for optimization of D + UTS

**Table 10:** Results of optimization and confirmatory tests

| | Response | Optimum input parametric levels | | | Predicted maximum response | Confirmatory test result | Error (%) |
|---|---|---|---|---|---|---|---|
| | | I (A) | F (lpm) | S (mm/s) | | | |
| RSM method | UTS | 83.43 | 10.45 | 2.0 | 528.94 MPa | 530.44 MPa | 0.28 |
| | Ductility | | | | 17.26 % | 16.80 % | 2.66 |
| PSO method | UTS | 77.12 | 11.07 | 2.00 | 530.825 MPa | 531.21 MPa | 0.07 |
| | Ductility | 100.0 | 9.00 | 2.00 | 18.6954 % | 18.60 % | 0.48 |

## 4. CONCLUSIONS

On the basis of laboratory results and analyses of the present investigation on TIG welding of AISI 420 martensitic stainless steel, few conclusions are drawn.

I) Successful homogeneous TIG welded joints can be made of this stainless steel by using preheating at 250°C temperature for 30 minutes.

ii) Most of the welded joints, under varied conditions of welding within the range of experiments, retain their strength and ductility.

iii) Response surface analysis is found to be suitable for mathematical modeling and response optimization.

iv) Metaheuristics are very efficient to maximize response outputs (i.e. UTS and ductility) and to find out corresponding optimum parametric combination of input

parameters: welding current, gas flow rate and welding speed.

v) Particle swarm optimization (PSO) is most efficient in finding the global maxima, as well as this technique converges faster than other metaheuristic methods. PSO, ESWSA, CS and FPA can reach global maxima whereas BA and GA stick to local maxima point for the case of UTS optimization.

vi) Confirmatory tests validate the proposed methodologies of parametric optimization of TIG welding by RSM method and different metaheuristic methods.

vii) Microstructural characteristics are also studied and interpreted; significance of the parameters has also been evaluated through ANOVA.

## REFERENCES


[1] Isfahany, A.N., Saghafian, H. and Borhani, G., The Effect of Heat Treatment on Mechanical Properties and Corrosion Behavior of AISI 420 Martensitic Stainless Steel, Journal of Alloys and Compounds, Vol. 509, pp.3931–3936, 2011.

[2] Davis, J.R., Corrosion of Weldments, ASM International, Materials Park, USA, 2006.

[3] Lippord, J.C. and Kotecki, D.J., Welding Metallurgy and Weldability of Stainless Steels, John Wiley & Sons, Inc., Hoboken, New Jersey, pp.56-86, 2005.

[4] Kose, C. and Kacar, R., The Effect of Preheat & Post Weld Heat Treatment on The Laser Weldability of AISI 420 Martensitic Stainless Steel, Materials and Design, Vol. 64, pp.221–226, 2014.

[5] Castro, R. and Cadenet, J.J., Welding Metallurgy of Stainless and Heat Resisting Steels, Cambridge University Press, London, pp.45-66, 2005.

[6] Baghjari, S.H. and Mousavi, S.A.A.A., Effects of Pulsed Nd:YAG Laser Welding Parameters and Subsequent Post-Weld Heat Treatment on Microstructure and Hardness of AISI 420 Stainless Steel, Materials and Design, Vol. 43, pp.1-9, 2013.

[7] Andrews, K.W., Empirical Formula for the Calculation of Some Transformation Temparatures, Journal of Iron Steel Institute, Vol. 203, pp.721-727, 1965.

[8] Shirmohammadi, D., Movahedi, M. and Pouranvari, M., Resistance Spot Welding of Martensitic Stainless Steel: Effect of Initial Base Metal Microstructure on Weld Microstructure and Mechanical Performance, Materials Science & Engineering A, Vol. 703, pp.154-161, 2017.

[9] Pouranvari, M., Fracture Toughness of Martensitic Stainless Steel Resistance Spot Welds, Materials Science & Engineering A, Vol. 680, pp.97-107, 2017.

[10] Kurt, B., Orhan, N., Somunkiran, I. and Kaya, M., The Effect of Austenitic Interface Layer on Microstructure of AISI 420 Martensitic Stainless Steel Joined by Keyhole PTA Welding Process, Materials and Design, Vol. 30, pp.661–664, 2009.

[11] Yılmaz, R. and Türkyılmazoglu, A., Tensile Properties of Martensitic Stainless Steel Weldments, Advanced Materials Research, Vol. 23, pp.319-322, 2007.

[12] Raja, D.J.E. and Dhas, S.J.H., A Review on Optimization of Welding Process, Procedia Engineering, Vol. 38, pp.544-554, 2012.

[13] Kiaee, N. and Aghaie-Khafri, M., Optimization of Gas Tungsten Arc Welding Process by Response Surface Methodology, Materials and Design, Vol. 54, pp.25–31, 2014.

[14] Gunaraj, V. and Murugan, N., Application of Response Surface Methodology for Predicting Weld Bead Quality in Submerged Arc Welding of Pipes, Journal of Materials Processing Technology, Vol. 88, pp.266–275, 1999.

[15] Elatharasana, G. and Senthil Kumar, V.S., An Experimental Analysis and Optimization of Process Parameter on Friction Stir Welding of AA 6061-T6 Aluminum Alloy Using RSM, Procedia Engineering, Vol. 64, pp.1227–1234, 2013.

[16] Benyounis, K.Y., Olabi, A.G. and Hashmi, M.S.J., Optimizing the Laser-Welded Butt Joints of Medium Carbon Steel Using RSM, Journal of Materials Processing Technology, Vol. 164–165, pp.986–989, 2005.

[17] Pasupathy, J. and Ravisankar, V., Parametric Optimization of TIG Welding Parameters Using Taguchi Method for Dissimilar Joint (Low Carbon Steel with AA1050), International Journal of Scientific & Engineering Research, Vol. 4, No.11, pp.25-28, 2013.

[18] Eşme, U., Application of Taguchi Method for the Optimization of Resistance Spot Welding Process, Arabian Journal for Science and Engineering, Vol. 34, No.2, pp.519-528, 2009.

[19] Nagesha, D.S. and Datta, G.L., Genetic Algorithm for Optimization of Welding Variables for Height to Width Ratio and Application of ANN for Prediction of Bead Geometry for TIG Welding Process, Applied Soft Computing, Vol. 10, pp.897–907, 2010.

[20] Sette, S., Boullart, L. and Langenhove, L., Optimizing a Production Process by a Neural Network/Genetic Algorithm Approach, Engineering Applications of Artificial Intelligence, Vol. 9, No. 6, pp.681-689, 1996.

[21] Satheesh, M. and Dhas, J.E.R., Multi Objective Optimization of Flux Cored Arc Weld Parameters Using Fuzzy Based Desirability Function, IJST Transactions of Mechanical Engineering, Vol. 37, pp.175-187, 2013.

[22] Yang, L.J., Bibby, M.J. and Chandel R.S., Linear Regression Equations for Modeling the Submerged-Arc Welding Process, Journal of Materials Processing Technology, Vol. 39, No.1-2, pp.33-42, 1993.

[23] Lee, J.I. and Rhee, S., Prediction of Process Parameters for Gas Metal Arc Welding by Multiple Regression Analysis, Proceedings of the Institution of Mechanical Engineers, Part B: Journal of Engineering Manufacture, Vol. 214, No.6, pp.443-449, 2000.

[24] Jamil, M. and Yang, X.S., A Literature Survey of Benchmark Functions for Global Optimization Problems, International Journal of Mathematical Modelling and Numerical Optimisation, Vol. 4, No.2, pp.150–194, 2013.

[25] Ghosh, A., Mandal, S., Nandi, G. and Pal, P.K., Metaheuristic Based Parametric Optimization of TIG Welded Joint, Transactions of the Indian Institute of Metals, Vol. 71, No.8, pp.1963–1973, 2018.

[26] Canyurt, O.E., Estimation of Welded Joint Strength Using Genetic Algorithm Approach, International Journal of Mechanical Sciences, Vol. 47, pp.1249–1261, 2005.

[27] Kim, D., and Rhee, S., Optimization of Arc Welding Process Parameters Using a Genetic Algorithm, Welding Journal, Vol.80, pp.184-189, 2001.

[28] Yang, X.S., A New Metaheuristic Bat-Inspired Algorithm, Proceeding of Nature Inspired Cooperative Strategies for Optimization, Vol. 284, pp.65-74, 2010.

[29] Mandal, S., Khan, A., Saha, G. and Pal, R.K., Reverse Engineering of Gene Regulatory Networks Based on S-Systems and Bat Algorithm, Journal of Bioinformatics and Computational Biology, Vol. 14, No.3, pp.1-22, 2010.

[30] Yang, X.S. and Deb, S., Engineering Optimisation by Cuckoo Search, International Journal of Mathematical Modelling and Numerical Optimisation, Vol. 1, No.4, pp.330–343, 2010.

[31] Mandal, S., Khan, A., Saha, G. and Pal, R.K., Large Scale Recurrent Neural Network Based Modeling of Gene Regulatory Network Using Cuckoo Search-Flower Pollination Algorithm, Advances in Bioinformatics, pp.1-9, 2016.

[32] Yang, X.S., Flower Pollination Algorithm for Global Optimization, Proceeding of Unconventional Computation and Natural Computation, Lecture Notes in Computer Science, Vol. 7445, pp.240-249, 2012.

[33] Yang, X.S., Karamanoglu, M. and He, X.S., Flower Pollination Algorithm: A Novel Approach for Multi-objective Optimization, Engineering Optimization, Vol. 46, No.9, pp.1222-1237, 2014.

[34] Eberhart, R.C. and Shi, Y.H., Comparing Inertia Weights and Constriction Factors in Particle Swarm Optimization, Proceeding of IEEE Congress on Evolutionary Computation, pp.84–88, 2000.

[35] Shi, Y.H. and Eberhart, R.C., Experimental Study of Particle Swarm Optimization, Proceeding of SCI 2000 Conference, Vol. 3, pp.1945-1950, 2000.

[36] Mandal, S., Elephant Swarm Water Search Algorithm for Global Optimization, Sadhana, vol. 43(2), pp. 1-21, 2018.

[37] Mandal, S., Saha, G. and Pal, R.K., Recurrent Neural Network Based Modeling of Gene Regulatory Network Using Elephant Swarm Water Search Algorithm, Journal of Bioinformatics and Computational Biology, Vol. 15, No.4, pp.1-23, 2017,

[38] Man, K.F., Tang, K.S. and Kwong, S., Genetic Algorithms: Concepts and Applications [In Engineering Design], IEEE Transactions on Industrial Electronics, Vol. 43, No.5, pp.519-534, 1996.

[39] Sathiya, P., Panneerselvam, K. and Jaleel, M.Y.A., Optimization of Laser Welding Process Parameters for Super Austenitic Stainless Steel Using Artificial Neural Networks and Genetic Algorithm, Materials and Design, Vol. 36, pp.490–498, 2012.

[40] Correia, D.S., Gonçalves, C.V., Cunhada, S.S. and Ferraresi Jr., V.A., Comparison Between Genetic Algorithms and Response Surface Methodology in GMAW Welding Optimization, Journal of Materials Processing Technology, Vol. 160, pp.70–76, 2005.

[41] Fitrianto, A. and Midi, H., Multi-response Optimization via Desirability Function for the Black Liquor Data, Journal of Science and Technology, pp.91–102, 2012.

[42] Mandal, S., Dutta, P. and Kumar, A., Modeling of Liquid Flow Control Process Using Improved Versions of Elephant Swarm Water Search Algorithm, SN Applied Science, Vol. 1, No.8, pp.1–15, 2019